# Oil biodegradation in permeable marine sediments: Effects of benthic pore-water advection and solute exchange

Xiaolong Geng[1, 2*], Christopher H. Barker[2], Amy MacFayden[2], Michel C Boufadel[3], Kenneth Lee[4], Dalina L. Thrift-Viveros[2], Robert Jones[2], and Caitlin O'Connor[2]

**Submitted to**

*Journal of Hazardous Materials:*

*Special Issue on Emerging Technologies for Marine Oil Spill Response*

[1]Genwest Systems, Inc, Edmonds, WA 98020, USA.

[2]Office of Response and Restoration, Emergency Response Division, National Oceanic and Atmospheric Administration, Seattle, WA 98133, USA.

[3]Department of Civil and Environmental Engineering, New Jersey Institute of Technology, University Heights, Newark, NJ 07102, USA.

[4]Department of Fisheries and Oceans, Dartmouth, Nova Scotia, B2Y4A2, Canada.

*: Corresponding Author, email: leo.geng@noaa.gov

**Abstract**

Oil spills have been recognized as among the worst kinds of environmental disasters, causing severe coastal ecological and economic damages. Although benthic flow and solute fluxes are known to have strong impacts on fate and transport of oil deposited within marine sediments, their endogenous mechanisms still remain to be uncovered. In this paper, simulations of flow and solute transport processes along with hydrocarbon biodegradation were conducted in a cylindrical benthic chamber system to investigate influences of benthic hydrodynamics on oil biodegradation in permeable marine sediments. Results show that ripple-flow interactions create subsurface recirculation cells whereby seawater infiltrates into the benthic sediments at ripple troughs while groundwater discharges near the crests. It results in a spatially varied oil biodegradation rate in marine sediments. Significant oil biodegradation occurs near sediment ripple troughs due to direct oxygen recharge, while biodegradation of oil deposited uphill becomes slow due to limited oxygen replenishment. Oil biodegradation decreases subsurface oxygen content, and consequently impedes discharge of oxygen from benthic sediments. Our results reveal a dynamic interaction between oil biodegradation and benthic flow and solute transport processes, which has strong implications for predicting oil persistence and biodegradation within marine sediments and its associated impacts on benthic biogeochemical processes.

## 1. Introduction

Oil spills pose severe threats to marine coastal areas worldwide, deteriorating shoreline environments and causing severe ecological and economic damage. The 1989 Exxon Valdez oil spill contaminated around 800 km of shorelines within Prince William Sound, Alaska [*Michel and Hayes*, 1999; *Short et al.*, 2004; *Boufadel et al.*, 2016]. In 2002, the Prestige oil spill occurred off the coast of Galicia, Spain, polluting over 600 sandy beaches along the Spanish Atlantic coast [*Fernández-Fernández et al.*, 2011; *Acosta-González et al.*, 2015]. The 2010 Deepwater Horizon oil spill led to the release of an estimated 3.19 million barrels of crude oil into the Gulf of Mexico and an estimated 22,000 tons of weathered oil washed up on northern Gulf of Mexico beaches [*Michel et al.*, 2013; *Boufadel et al.*, 2014; *Geng et al.*, 2021a]. Incidents of these magnitudes resulted in serious consequences on marine ecosystems, degrading abundance and diversity of benthic communities [*Glemarec and Hussenot*, 1981; *Teal and Howarth*, 1984]. The toxicity in oils is primarily from aromatic hydrocarbons, particularly polycyclic aromatic hydrocarbons (PAHs) [*Neff*, 2002]. Marine organisms are found to be affected by PAHs at every life stage, from free floating embryos and larvae to sexually mature adults [*Adzigbli and Yuewen*, 2018], and across species types. For instance, crustaceans can be exposed to oil through digging into oiled sediments, ingestion with food, and direct interaction [*Cormack et al.*, 2011; *Montagna et al.*, 2013], and often experience high mortality after oil spills [*McCay et al.*, 2001]. *Bodkin et al.* [2012] reported consequent impacts of the Exxon Valdez oil spill on the decrease in sea otter subpopulation rate in the heavily oiled northern Knight Island area of Prince William Sound. *Reuscher et al.* [2017] investigated impacts of the Deepwater Horizon oil spill on benthic infauna of the northern Gulf of Mexico continental slope. Their study found that oil originating from the Deepwater Horizon reached the seafloor and had a persistent negative impact on diversity of soft-bottom, deep-sea benthic communities. While signs of recovery for some benthic community

variables are shown, full recovery had not yet occurred even four years after the spill.

There are various driving mechanisms that can cause sedimentation of spilled oil onto nearshore and benthic sediments [*Teal and Howarth*, 1984; *Boufadel et al.*, 2019]. Mixing of spilled oil with sediments often occurs in shallow water by breaking waves and further transport to deeper water is driven by subsequent currents (Figure 1A) [*Owens and Lee*, 2003; *O'Laughlin et al.*, 2017]. Oil could also attach onto particulate matter suspended in the water column and subsequently sink in deeper water [*Gong et al.*, 2014; *Shan et al.*, 2020]. Pore-water advection within marine sediments is often generated by the pressure gradients at the sediment surface that occur when bottom current flow is deflected by topographical structures such as mounds or ripples [*Huettel and Gust*, 1992; *Janssen et al.*, 2005a]. It has been proven to play a critical role in biogeochemical processes in marine benthic sediments, including carbon mineralization, nutrient recycling, and recycled primary production [*Janssen et al.*, 2005a; *Geng et al.*, 2021b]. Tracer studies illustrated that ripple-flow interactions generate groundwater recirculation cells in marine sediments with flows infiltrating in the ripple troughs and exfiltrating from crests (Figure 1B) [*Webb and Theodor*, 1968; *Shum*, 1992]. Such seawater-groundwater recirculation brings organic matter and oxygen into the sediment, creates horizontal concentration gradients that can be as strong as the vertical gradients, and provides an important mechanism for enhancing mineralization of organic matter in marine sediments [*Huettel et al.*, 1998]. Although advective flow and solute fluxes across the water-sediment interface could have strong impacts on fate and transport of oil deposited within marine sediments, endogenous mechanisms of benthic flow and solute exchange interacting with oil biodegradation in marine sediments have not been investigated yet.

Investigation of benthic flow and solute exchange has been widely performed with benthic

chambers. Experiments involve benthic stirred chambers where the centrifugal-force-induced pressure gradients at the sediment surface generate pore-water advection that circulates the overlying water through the sediment [*Tengberg et al.*, 1995; *Glud et al.*, 1996], and benthic landers deployed to the sea floor for direct in-situ measurements and observations [*Black et al.*, 2001; *D'Onghia et al.*, 2018]. Mathematical modeling has also been widely used to investigate flow and solute transport processes within benthic sediments. It allows us to interpret measurement data collected from experiments and examine complex field-like conditions which are difficult to reproduce with laboratory experiments. *Khalili et al.* [1997] and [1999] derived a numerical solution of the Darcy-Brinkmann-Lapwood equation to characterize the axisymmetric advective flow in a cylindrical chamber system. Calculations were performed to quantify the flow exchange between the permeable sediment and the overlying water. *Meysman et al.* [2007] conducted numerical simulations to investigate biologically and physically induced flow and tracer dynamics in marine benthic sediments. In their study, the finite element package COMSOL Multiphysics$^{TM}$ 3.2a was used to develop flow and reactive transport models for characterizations of advective flow and associated fluxes across the sediment-water interface. While considerable efforts have been made on modeling benthic flow and solute exchange processes, interactions between coastal benthic exchange dynamics and oil biodegradation have not been numerically conducted within benthic oil-contaminated sediments.

The objective of this paper is to investigate interactions between benthic oil biodegradation and pore-water advection along with solute exchange in marine sediments. We developed a two-dimensional (2D) flow and reactive transport model in cylindrical coordinates for the investigation. The development was based on transformation of our prior developed BIOMARUN model from Cartesian to cylindrical coordinates. We conducted simulations of

groundwater flow, reactive transport of oxygen and a nutrient (nitrogen), and hydrocarbon biodegradation in a cylindrical benthic sediment chamber to characterize the patterns of microbial degradation of oil subjected to benthic flow and solute flux exchange across the water-sediment interface. Particle tracking was further performed to analyze advective flow paths and associated travel time in this chamber system. The results highlight the important role of benthic hydrodynamics in hydrocarbon biodegradation within permeable marine sediments.

## 2. Methods

### *2.1 BIOMARUN model in cylindrical coordinates*

The BIOMARUN model in Cartesian coordinates has been developed and validated in our prior studies [*Geng et al.*, 2015; *Geng et al.*, 2016; *Geng et al.*, 2017a]. The model couples the MARUN model [*Boufadel et al.*, 1999; *Geng and Boufadel*, 2017; *Geng et al.*, 2020], a 2-D finite element model considering density-dependent flow and solute transport in variably saturated media, with the BIOB model, a multiplicative Monod model for hydrocarbon biodegradation [*Geng et al.*, 2013; *Geng et al.*, 2014a]. In this paper, we transformed the BIOMARUN model from Cartesian coordinates to cylindrical coordinates, named CYL-BIOMARUN, to simulate benthic flow and solute transport processes in a cylindrical chamber system. The equation for the conservation of water is written as:

$$\frac{\partial(\beta\phi S)}{\partial t} = \frac{1}{r}\frac{\partial(\mathrm{r}\,\beta K_r \frac{\partial \psi}{\partial r})}{\partial r} + \frac{\partial(\beta K_z \frac{\partial \psi}{\partial z})}{\partial z} + \frac{\partial(\beta^2 K_z)}{\partial z}, \quad (1)$$

where $\beta$ is the density ratio [-] defined as the ratio of salt-dependent water density to freshwater density [$ML^{-3}$]; $\phi$ is porosity [-], $S$ is soil moisture ratio [-], $\psi$ is pressure head [L], and $K_r$ and $K_z$ are radial and vertical freshwater hydraulic conductivities.

154

155 The conservative solute (e.g., salt) transport equation can be expressed as:

$$\phi S\frac{\partial c_0}{\partial t}=\beta\phi S\frac{(D_{rr}\frac{\partial c_0}{\partial r}+D_{rz}\frac{\partial c_0}{\partial z})}{r}+\beta\nabla\cdot(\phi S\vec{D}\cdot\nabla c_0)-\vec{q}\cdot\nabla c_0, \quad (2)$$

156 where $c_0$ is concentration, and $\vec{q}$ is Darcy flux vector given by:

$$\vec{q}=(q_r,q_z)=-(K_r\frac{\partial\psi}{\partial r},K_z\frac{\partial\psi}{\partial z}+\beta), \quad (3)$$

157 The term $\vec{D}$ represents physical dispersion tensor written as

$$\vec{D}=\frac{1}{\|\vec{q}\|}\begin{pmatrix}\alpha_L q_r^2+\alpha_T q_z^2 & (\alpha_L-\alpha_T)q_r q_z\\ (\alpha_L-\alpha_T)q_r q_z & \alpha_T q_r^2+\alpha_L q_z^2\end{pmatrix}, \quad (4)$$

158 where $\|\vec{q}\|=\sqrt{q_r^2+q_z^2}$, $\alpha_L$ and $\alpha_T$ are longitudinal and transverse dispersivities (L),

159 respectively.

160 The reactive solute transport equation can be expressed as:

$$\phi SR_i\frac{\partial c_i}{\partial t}=\beta\phi S\frac{(D_{rr}\frac{\partial c_i}{\partial r}+D_{rz}\frac{\partial c_i}{\partial z})}{r}+\beta\nabla\cdot(\phi S\vec{D}\cdot\nabla c_i)-\vec{q}\cdot\nabla c_i+\phi DR_i r_i, \quad (5)$$

161 where $R_i$ is the retardation coefficient of $i_{\text{th}}$ solute $c_i$; $r_i$ is a reaction rate representing

162 generation or consumption. Six reactive components of two types of oil components (alkanes

163 and polycyclic aromatic hydrocarbons (PAHs)), their corresponding microbial degraders,

164 dissolved oxygen and a nutrient (nitrogen) are considered. The reaction network of these six

165 components is consistent with the BIOB model, where in general microbes consume

166 dissolved oxygen and nutrients for degrading oil compounds following modified Monod

167 kinetics. For example, the growth coefficient of microbial degraders, $\mu_i$, can be expressed as

168 follows:

$$\mu_i = \mu_{\max}(1-\frac{X_i}{X_{\max}})(\frac{S_i}{K_S+S_i})(\frac{N}{K_N+N})(\frac{O^4}{K_O+O^4}) \quad (6)$$

Where $i$ = 1 and 2, denoting alkane and PAH degraders, respectively, and $\mu_{max}$ represents maximum growth coefficients ($day^{-1}$). The parameters $S_i$, $N$, and $O$ represent concentrations of substrate, nutrient, and oxygen. The parameters $K_S$ and $K_N$ represent the half-saturation concentrations for substrate and nitrogen, respectively (see *Geng et al.* [2014a] and [2015] for details). The CYL-BIOMARUN model was validated by reproducing the experimental results measured in *Khalili et al.* [1999] (Figure 2).

*2.2 Numerical simulations of oil biodegradation in a benthic chamber system*

The simulated domain was constructed in a cylindrical coordinate system with the radius length of 50 cm and height of 100 cm, representing a cylindrical benthic chamber system. A mesh of 2278 nodes (34 nodes in the radial and 67 nodes in the vertical) was used, resulting in ~1.5 cm spatial resolution. The mesh was made fine enough to meet the criterion for the grid Peclet number to be less than or equal to 2.0 [*Zheng and Bennett*, 2002]. For the flow simulation, a steady-state radial-symmetric pressure distribution was applied at the top boundary of the domain (Figure 3A). This boundary condition is commonly used for simulating the chamber system where the sediment-water interface is flat, and a radial-symmetric stirring pattern establishes in the overlaying water [*Glud et al.*, 1996]. For fate and transport simulations, a Dirichlet boundary condition was used at the top boundary, and a Neumann boundary condition with zero dispersive flux was assigned to the rest of the boundaries. The initial concentration of dissolved oxygen and nutrients was assumed to be 6.0 mg/L and 1.0 mg/L in sediments, and 1.2 mg/L and 0.2 mg/L in seawater, respectively. To model microbial degradation of oil, the oil composition can be modeled as pseudo-components with distinct mass fractions and biodegradation rate [*Thrift-Viveros et al.*, 2015].

For simplification, the oil was assumed to be composed of two major groups, long-chain alkanes and polycyclic aromatic hydrocarbons (PAHs), deposited within the top 5 cm of sediments. The concentrations of alkanes and PAHs were assigned as 4.0 mg/kg of sediment and 2.0 mg/kg of sediment, respectively (Figure 3B).

For all the simulations, the numerical model was first run for approximately 100 days without oil deposition until the hydraulic and hydrodynamic regime reached a steady state. The pressure and solute distributions were then used as initial conditions for the simulation with oil contamination near the sediment surface, which ran over a simulation time of 300 days. The time step was selected at 10.0 s, resulting in a grid Courant number less than 0.9 (a value less than 1.0 is required). The parameter values adopted in the simulations are reported in Table 1. Backward particle tracking was performed to reveal the flow pathways and associated travel time. A particle tracking code, named NEMO-3D, based on the random walk particle tracking algorithm was used [*Geng et al.*, 2014b; *Geng et al.*, 2017b; *Geng et al.*, 2020]. The neutrally buoyant particles were released at a 5-cm interval along the sediment surface, driven by the flow fields obtained from the CYL-BIOMARUN simulation.

## 3. Results

### *3.1 Comparison with the experiment data of Khalili et al. [1999]*

*Khalili et al.* [1999] conducted experiments to investigate recirculating flow through benthic fluid-sediment interfaces. The experimental set-up is a stationary cylinder that contains a fluid-saturated porous medium with supernatant water on top. The recirculating flow was generated by deploying a rotating lid in the upper fluid region, and further characterized by monitoring dye washout from the sediment. Dye transport was visualized using positron emission tomography (PET), a non-invasive technique which allows to see through an

opaque solid matrix, and to obtain full 3-D pictures of washing out dye from the sediment. In their study, digital photographic visualization and associated image processing were also performed to further quantify the near-wall dye-washout depth. Figure 2A shows a comparison of normalized radioactivity strength measured at different times by PET along with numerical results obtained by CYL-BIOMARUN model and the model developed in *Basu and Khalili* [1999]. As shown in the figure, the CYL-BIOMARUN model reasonably captures the dye transport within the sediment column. The results of washout depth show that both numerical models underestimate the first half-hour washout of dye from the sediment (Figure 2B). This is most likely due to the loss of some dye from the sediment to the fluid layer when the experiments were initialized, which was not considered in the numerical simulations.

### *3.2 Simulations of pore-water advection, solute exchange, and oil biodegradation in a benthic chamber system*

Surface pressure gradients have a strong influence on flow and transport processes within benthic sediments. Figure 3A shows that the pressure gradients imposed along the sediment surface alter subsurface pressure distribution, creating a high-pressure zone at the outer ring of the chamber and relatively low-pressure zone in the proximity of the chamber center. The resulting pressure differences transmit through the subsurface and generate pressure gradients in both radial and vertical directions. The penetration depth is approximately 20 cm for the simulations considered in this paper. Figures 3C and 3D show that an upper plume is generated in the subsurface with seawater-derived chemical properties that are distinguished from ambient groundwater. This is expected as the formation of the plume is due to seawater infiltration. The plume has a deeper expansion beneath the high-pressure zone, and becomes shallower as it moves to the relatively low-pressure zone. The concentration of oxygen

gradually decreases from 6.0 mg/L to 1.0 mg/L and concentration of nutrients gradually increases from 0.2 mg/L to 1.2 mg/L in the proximity of the plume edge, indicating substantial mixing between seawater and groundwater in benthic sediments. The steady-state simulations show the maximum washout depth by seawater is ~20 cm while the thickness of the seawater-groundwater mixing zone is ~25 cm.

Particle tracking results show the pressure gradients create a recirculation cell whereby seawater infiltrates into the benthic sediments through the high-pressure zone and groundwater discharge occurs along the low-pressure zone (Figure 4). Figure 4A shows the advective flow pathways within the recirculation cell simulated by a backward particle tracking scheme. Infiltration flow occurs near the outer ring of the chamber between R = 40 cm and 50 cm, while exfiltration flow is present at the inner part of the chamber between R = 0 and 40 cm. The particles migrating along deeper flow paths experience longer travel time (Figure 4B). In particular, the travel time of the particles discharged near the location of R = 2 cm is about 100 years. The particles' travel time drops exponentially as their discharge locations get close to the infiltration zone due to shorter flow paths.

Oil biodegradation demonstrates a large spatial variation in benthic sediments. The concentration contour of alkanes shows that two biodegradation hotspots appear in the oiled sediment layer after 30 days near the top within the infiltration zone and near the bottom within the exfiltration zone, respectively (Figure 5A). The spatial extent of these two hotspots gradually expands with time (e.g., time t = 60 days and 100 days). After 300 days, nearly all the alkanes deposited within these two hotspots are biodegraded. In contrast, a considerable amount of alkanes still remains near the middle ring of the chamber. Similar tempo-spatial patterns are observed for PAHs as well but at much lower biodegradation rate (Figure 5B).

Compared to alkanes, biodegradation of PAHs is negligible within the first 100 days. After 300 days, biodegradation of PAHs is around 15% near its hotspots, and negligible at other locations. Oil biodegradation greatly alters benthic oxygen conditions (Figure 5C). After 30 days, the near-surface oxygen level significantly drops within the exfiltration zone to a concentration less than 1.0 mg/L, resulting in anoxic conditions for oil biodegradation. The oxygen level beneath the oiled sediment layer gradually decreases with time, due to large oxygen consumption from the upper oiled layer. In contrast, the oxygen content within the infiltration zone always remains above 2.0 mg/L, which provides a favorable aerobic condition for oil biodegradation. This is most likely because direct recharge of oxygen-rich seawater to some extent compensates for the oxygen consumption there. Compared to oxygen, the nutrient (nitrogen) condition remains at its original level. This is probably due to recycling of nutrients during the oil biodegradation processes (Figure 5D). On the one hand, oil degraders consume nitrogen for microbial growth, but on the other hand, they release nitrogen during their endogenous decay.

Figure 6A reports the alkane biodegradation at three different radial locations. As expected, the highest biodegradation rate is observed at the outer ring of the chamber (i.e., R = 45 cm), where above 98% of alkanes are biodegraded after 300 days. The biodegradation rate tends to be lower as it moves to the inner side (i.e., R = 15 cm), where alkanes are biodegraded about 80% after 300 days. The lowest alkane biodegradation occurs near the mid-ring location (i.e., R = 30 cm); nearly 10% of alkanes are biodegraded within the first 20 days, and then the biodegradation rate dramatically drops. Similar tempo-spatial patterns are also observed for PAHs at a much lower rate. This is consistent with tempo-spatial variation of oxygen level within the benthic sediment (Figure 6C). The oxygen concentration demonstrates a sudden decrease after the oil deposition. In particular, the oxygen concentration drops below 2 mg/L

292 at locations R = 15 cm and 30 cm, indicating anoxic environments there for oil
293 biodegradation. In contrast, oxygen concentration at location R = 45 cm only drops down to
294 4.5 mg/L and then recovers back to 5.5 mg/L after 300 days.
295
296 Figure 7 reports the percentage (%) loss of alkanes and PAHs at different radial locations.
297 Obviously, the % loss is the largest near the outer ring of the chamber (i.e., between R = 40
298 cm and 50 cm), which is about 100% and 20% for alkanes and PAHs, respectively.
299 Comparable loss of alkanes and PAHs is found at the zone between R = 5 cm and 15 cm.
300 The % loss drops as it moves to the middle ring of the chamber, reaching the minimum at R =
301 30~35 cm, which is about 35% and 5% for alkanes and PAHs, respectively. The minimum
302 loss is also observed at the center of the chamber (i.e., between R = 0 and 5 cm), which is
303 probably due to persistent low oxygen content there.
304
305 Pore-water advection significantly affects oil biodegradation in benthic sediments. The pore-
306 water velocity contour shows a higher magnitude near the surface at the outer and inner ring
307 of the chamber (Figure 8A). Interestingly, it is inconsistent with the magnitude of pressure
308 imposed at the sediment surface, which gradually decreases along the radial direction from
309 the outer ring boundary to the inner center of the chamber. This is due to the fact that the
310 intensity of pore-water flow is determined by the pressure gradient rather than pressure itself.
311 Figures 8B and 8C show exchange flux and flow across the sediment surface, respectively.
312 Seawater infiltration occurs near the outer ring of the chamber between R = 40 cm and 50 cm,
313 showing the largest rate at the chamber edge. In contrast, groundwater discharge occurs at the
314 inner part of the chamber between R = 0 to 40 cm, reaching the highest rate at R = 25 cm.
315 Although the majority of groundwater discharge appears near the middle ring of the chamber,
316 discharge flux tends to be the largest near the inner center of the chamber (i.e., R = 5 cm),

and gradually decreases as the radius increases. It indicates a relatively poor hydraulic exchange at the middle ring of the chamber, which to some extent explains the relatively low oil biodegradation rate there.

The interactions between benthic solute exchange and biodegradation of deposited oil in benthic sediments are dynamic. Figure 9A shows the temporospatial evolution of oxygen exchange across the water-sediment interface after the oil deposition. Although there is a steady oxygen recharge into the benthic sediments, the oxygen exchange curves tend to be flat at 0.0 mg/h along the entire discharge zone following the oil deposition (e.g., at time t =10 days and 100 days). It indicates that oil deposition impedes discharge of oxygen from the benthic sediments due to its large consumption for hydrocarbon biodegradation. The positive discharge of oxygen starts to occur again after 300 days of the oil deposition at locations between R = 30 cm and 40 cm which is in proximity of the oxygen recharge zone. It indicates that the oxygen concentration is returned to its initial levels by seawater infiltration after major amounts of oil are removed by biodegradation along the discharge flow paths. Figure 9B shows the temporospatial evolution of oxygen flux at the bottom of the oiled layer (i.e., Z = 95 cm). The oxygen replenishment along the entire bottom of the oiled sediment layer largely decreases within the first 100 days following the deposition, particularly next to the infiltration zone between R = 30 cm and 40 cm. This is due to the oxygen consumption at the infiltration zone, diminishing the replacement of oxygen downstream. Such oxygen depletion has lesser impacts on farther discharge locations (e.g., between R = 5 cm and R = 30 cm) due to the following reasons: 1) initial oxygen storage within benthic sediments provides additional oxygen replenishment for downstream oil biodegradation, and 2) the higher water and oxygen flux at the farther discharge locations. The intensity of oxygen replenishment is consistent with the magnitude of oil biodegradation within the benthic sediments, indicating

342 the importance of solute (i.e., oxygen) exchange in biodegradation of deposited oil in benthic
343 sediments.
344

345 **4. Discussion**

346 Our results reveal a significant role of benthic flow advection and solute exchange in the fate
347 of oil deposited within permeable marine sediments. Pore-water advection has been
348 recognized as one of the most important drivers for benthic biogeochemical processes
349 [*Janssen et al.*, 2005b; *Cook et al.*, 2007; *Rocha*, 2008]. Our simulation results indicate that
350 bottom current flows deflected by topographical sediment structures will create subsurface
351 pore-water recirculation cells whereby seawater infiltrates into sediment ripple troughs while
352 groundwater discharges near the crest. It leads to a dynamic hydraulic and biogeochemical
353 environment for hydrocarbon biodegradation in benthic sediments. At sediment troughs, the
354 determinants of oil biodegradation rate are infiltration rate and biogeochemical properties of
355 seawater, while biodegradation of oil deposited near the sediment crest is primarily controlled
356 by upwelling groundwater flux beneath the exfiltration zone. Therefore, oil deposited within
357 marine sediments demonstrates spatially different biodegradation rates. Faster oil
358 biodegradation occurs in sediment ripple troughs due to direct and sufficient oxygen recharge
359 by seawater infiltration. In contrast, biodegradation of oil deposited uphill is slow and even
360 anoxic (i.e., extremely slow). Such spatial variations will increase the level of challenge to
361 assess oil spill contamination in marine sediments solely based on field measurements. This
362 is because random selection of oil-contaminated sediment samples might cause large
363 variability of oil measurements as natural attenuation of oil behaves differently in marine
364 sediments, depending on local topographic and flow patterns. Our results suggest that
365 characterization of sediment topographic properties and hydraulic conditions at sampling
366 locations are essential for thorough data interpretation and assessment of oil spills

367 contaminating marine sediments.

368

369 Dissolved oxygen and nutrients are key factors affecting hydrocarbon biodegradation; limited
370 availability of either could slow down the biodegradation rate considerably [*Passow and*
371 *Overton*, 2021; *Wang et al.*, 2021]. It has been observed that dissolved oxygen concentration
372 affects aerobic microbial growth in a sharp way [*Borden and Bedient*, 1986; *Borden et al.*,
373 1986; *Chiang et al.*, 1989]. The optimal oxygen concentration for microbial activities to
374 support aerobic oil biodegradation is 2.0-3.0 mg/L, above which increasing the oxygen
375 concentration does not enhance the microbial activities. However, when the concentration
376 drops below 2.0 mg/L, microbial activity switches sharply from aerobic to anaerobic in a way
377 that dramatically decreases oil biodegradation rate. Seawater infiltration into marine
378 sediments has been found to provide a major source of dissolved oxygen that enhances
379 sedimentary respiration as well as hydrocarbon biodegradation [*Anschutz et al.*, 2009; *Santos*
380 *et al.*, 2009]. Our results demonstrate that pore-water advection provides a critical control on
381 benthic solute (e.g., oxygen and nutrients) exchange. Ripple-flow interactions generate an
382 oxygen-rich plume beneath the benthic sediment surface, which has strong implications on
383 the fate and biodegradation of oil deposited in marine sediments. It likely creates an oxygen-
384 rich environment (i.e., above 2 mg/L) at ripple troughs that is favorable for aerobic oil
385 biodegradation. In contrast, oil biodegradation becomes slow and even anoxic near the ripple
386 crests because of the fact that oxygen is primarily consumed by oil biodegradation near the
387 recharge zone (i.e., ripple troughs) which reduces downstream oxygen replenishment. Our
388 results also show that oil deposition restructures benthic oxygen conditions. Oil
389 biodegradation reduces subsurface oxygen content, and consequently impedes discharge of
390 oxygen from the water-sediment interface. Such change could have long-term impacts on
391 benthic microbial community structures which have a large potential to alter nitrogen

dynamics, especially inorganic nitrogen release and denitrification processes [*Giblin et al.*, 1995; *Werner et al.*, 2006].

## 5. Conclusion

In this paper, we conducted numerical simulations of flow and solute transport processes and hydrocarbon biodegradation in a cylindrical benthic chamber system to investigate influences of benthic flow and solute exchange on oil biodegradation in marine sediments. Our results show that ripple-flow interactions create subsurface recirculation cells whereby seawater infiltrates into the benthic sediments through ripple troughs while groundwater discharges near ripple crests. It leads to spatially varied oil biodegradation rate in marine sediments, depending on local topographic and flow patterns. Significant oil biodegradation will occur in sediment ripple troughs due to direct and sufficient oxygen recharge by seawater infiltration. In contrast, biodegradation of oil deposited uphill is slow and under anoxic condition where oxygen replenishment is prohibited. Overall, this study reveals endogenous mechanisms within permeable benthic sediments that affect persistence and biodegradation of the deposited oil. It highlights the importance of benthic flow advection and solute exchange on characterizing fate of oil after its deposition within marine sediments. In particular, benthic flow recirculation along with solute exchange (e.g., oxygen and nutrients) creates a highly dynamic environment that increases spatial variability of oil decomposition within marine sediments. In coastal environments, permeability of sediments is heterogeneous, which could strongly alter magnitude and pathways of pore-water flows. In addition, relatively low temperature and high pressure in deep ocean could play an important role in benthic oil biodegradation there. These factors are not considered in current work, which are essential and need to be included in future studies.

## Acknowledgment

This work was funded by the US NSF (Division of Earth Sciences [EAR] #2130595. However, it does not necessarily reflect the views of the funding agency, and no official endorsement should be inferred.

## Figure Captions

**Figure 1.** Schematic of oil deposition and benthic exchange processes within permeable marine sediments. Note that the pressure gradients generated by ocean currents over ripples create circulation cells in marine sediments with flows infiltrating in the ripple troughs and exfiltrating from crests.

**Figure 2.** (A) a comparison of normalized radioactivity strength measured by PET (gray-scale filled contours) in Khalili et al., (1999) with numerical results obtained from Basu and Khalili (1999) and CYL-BIOMARUN model at different times. The dashed and solid curves represent the simulated radioactivity of 0.5 and 0.9, respectively. (B) A comparison of washout depths obtained from experiments and numerical simulations. Note that in order to compensate for the effect of premixing (i.e., observed loss of some dye from the sediment to the fluid layer at the initial instant of the experiments) in the experiments, Khalili et al., (1999) shifted back their numerical results by 12 minutes for additional comparison, plotted as a dashed line.

**Figure 3.** Simulated steady-state distributions of (A) pressure, (C) dissolved oxygen, and (D) nutrient (i.e., nitrogen) in the benthic chamber system. (B) Initial oil (i.e., alkanes and PAHs) distribution in the benthic sediment. In Figure 3A, the upper panel shows the pressure distribution along the water-sediment interface, and the lower panel shows steady-state pressure increment (above 100 cm) built by pressure gradients imposed at the water-sediment interface.

**Figure 4.** (A) Simulated flow paths of the particles released at 0.1-m interval along the sediment surface from R = 2 cm to 50 cm. (B) Travel time of the particles. Note that backward particle tracking was used to track advective flow paths. The start and end locations of particle flow paths are marked with blue symbols and a red line, respectively.

**Figure 5.** Simulated concentration contours of (A) alkanes, (B) PAHs, (C) oxygen, and (D) nutrient at different times. The dashed contour lines for alkanes and PAHs represent 75% and 95% of its initial concentration, respectively. The threshold of 2.0 mg/L that supports aerobic oil biodegradation is marked in oxygen contours. The nutrient contours demonstrate a negligible change with time; therefore, only its 300-day concentration contour is shown herein.

**Figure 6.** Temporal change of concentration for (A) alkanes, (B) PAHs, and (C) dissolved oxygen at three different radial locations (Z = 97.5 cm, and R = 15 cm, 30 cm, and 45 cm). The output locations are marked in the upper panel using the same color as the concentration curves.

**Figure 7.** Percentage loss of (A) alkanes and (B) PAHs at different radial locations.

**Figure 8.** (A) Simulated pore-water velocity field. The spatial distribution of (B) exchange flux ($cm^3/h \cdot cm^2$) and (C) exchange flow ($cm^3/h$) along the sediment-water interface. In Figure 8A, the color contour and uniform vectors represent magnitude and direction of pore water flow, respectively.

**Figure 9.** (A) Oxygen exchange across the water-sediment interface. (B) Oxygen flux across bottom of the oiled layer (i.e., Z = 95 cm). Note that the positive and negative values represent upward and downward flow directions, respectively.

## References


Acosta-González, A., S.-M. Martirani-von Abercron, R. Rosselló-Móra, R.-M. Wittich, and S. Marqués (2015), The effect of oil spills on the bacterial diversity and catabolic function in coastal sediments: a case study on the Prestige oil spill, *Environmental Science and Pollution Research*, *22*(20), 15200-15214.

Adzigbli, L., and D. Yuewen (2018), Assessing the impact of oil spills on marine organisms, *J. Oceanogr. Mar. Res*, *6*(179), 472-479.

Anschutz, P., T. Smith, A. Mouret, J. Deborde, S. Bujan, D. Poirier, and P. Lecroart (2009), Tidal sands as biogeochemical reactors, *Estuarine, Coastal and Shelf Science*, *84*(1), 84-90.

Basu, A., and A. Khalili (1999), Computation of flow through a fluid-sediment interface in a benthic chamber, *Physics of Fluids*, *11*(6), 1395-1405.

Black, K. S., G. R. Fones, O. C. Peppe, H. A. Kennedy, and I. Bentaleb (2001), An autonomous benthic lander:: Preliminary observations from the UK BENBO thematic programme, *Continental Shelf Research*, *21*(8-10), 859-877.

Bodkin, J. L., B. E. Ballachey, H. A. Coletti, G. G. Esslinger, K. A. Kloecker, S. D. Rice, J. A. Reed, and D. H. Monson (2012), Long-term effects of the 'Exxon Valdez'oil spill: sea otter foraging in the intertidal as a pathway of exposure to lingering oil, *Marine Ecology Progress Series*, *447*, 273-287.

Borden, R. C., and P. B. Bedient (1986), Transport of dissolved hydrocarbons influenced by

493 oxygen-limited biodegradation: 1. Theoretical development, *Water Resources Research*,
494 *22*(13), 1973-1982.
495 Borden, R. C., P. B. Bedient, M. D. Lee, C. H. Ward, and J. T. Wilson (1986), Transport of
496 dissolved hydrocarbons influenced by oxygen-limited biodegradation: 2. Field application,
497 *Water Resources Research*, *22*(13), 1983-1990.
498 Boufadel, M., X. Geng, C. An, E. Owens, Z. Chen, K. Lee, E. Taylor, and R. C. Prince
499 (2019), A Review on the Factors Affecting the Deposition, Retention, and Biodegradation of
500 Oil Stranded on Beaches and Guidelines for Designing Laboratory Experiments, *Current*
501 *Pollution Reports*, 1-17.
502 Boufadel, M. C., A. Abdollahi-Nasab, X. Geng, J. Galt, and J. Torlapati (2014), Simulation
503 of the landfall of the Deepwater Horizon oil on the shorelines of the Gulf of Mexico,
504 *Environmental science & technology*, *48*(16), 9496-9505.
505 Boufadel, M. C., X. Geng, and J. Short (2016), Bioremediation of the Exxon Valdez oil in
506 Prince William sound beaches, *Marine pollution bulletin*, *113*(1-2), 156-164.
507 Boufadel, M. C., M. T. Suidan, and A. D. Venosa (1999), A numerical model for density-
508 and-viscosity-dependent flows in two-dimensional variably saturated porous media, *Journal*
509 *of Contaminant Hydrology*, *37*(1-2), 1-20.
510 Chiang, C., J. Salanitro, E. Chai, J. Colthart, and C. Klein (1989), Aerobic biodegradation of
511 benzene, toluene, and xylene in a sandy aquifer—data analysis and computer modeling,
512 *Groundwater*, *27*(6), 823-834.
513 Cook, P. L., F. Wenzhöfer, R. N. Glud, F. Janssen, and M. Huettel (2007), Benthic solute
514 exchange and carbon mineralization in two shallow subtidal sandy sediments: Effect of
515 advective pore-water exchange, *Limnology and Oceanography*, *52*(5), 1943-1963.
516 Cormack, C. D., J. A. Hale, J. J. Gabriel, and O. Langman (2011), Nasima and Oil–Do They
517 Mix? Assessing Crab Survival in Oiled Sediments, paper presented at Proceedings
518 international oil spill conference. API, Washington, DC.
519 D'Onghia, G., F. Capezzuto, R. Carlucci, A. Carluccio, P. Maiorano, M. Panza, P. Ricci, L.
520 Sion, and A. Tursi (2018), Using a benthic lander to explore and monitor vulnerable
521 ecosystems in the Mediterranean Sea, *Acta Imeko*, *7*(2), 45-49.
522 Fernández-Fernández, S., A. Bernabeu, F. Bouchette, D. Rey, and F. Vilas (2011), Beach
523 morphodynamic influence on long-term oil pollution: The Prestige oil spill, *Journal of*
524 *Coastal Research*, 890-893.
525 Geng, X., C. Abou Khalil, R. C. Prince, K. Lee, C. An, and M. C. Boufadel (2021a),
526 Hypersaline pore water in Gulf of Mexico beaches prevented efficient biodegradation of
527 Deepwater Horizon beached oil, *Environmental science & technology* accepted.
528 Geng, X., and M. C. Boufadel (2017), The influence of evaporation and rainfall on supratidal
529 groundwater dynamics and salinity structure in a sandy beach, *Water Resources Research*,
530 *53*(7), 6218-6238.
531 Geng, X., M. C. Boufadel, and F. Cui (2017a), Numerical modeling of subsurface release and
532 fate of benzene and toluene in coastal aquifers subjected to tides, *Journal of Hydrology*, *551*,
533 793-803.
534 Geng, X., M. C. Boufadel, K. Lee, S. Abrams, and M. Suidan (2015), Biodegradation of
535 subsurface oil in a tidally influenced sand beach: Impact of hydraulics and interaction with
536 pore water chemistry, *Water Resources Research*, *51*(5), 3193-3218.

Geng, X., M. C. Boufadel, Y. R. Personna, K. Lee, D. Tsao, and E. D. Demicco (2014a), BioB: a mathematical model for the biodegradation of low solubility hydrocarbons, *Marine pollution bulletin*, *83*(1), 138-147.

Geng, X., M. C. Boufadel, H. Rajaram, F. Cui, K. Lee, and C. An (2020), Numerical study of solute transport in heterogeneous beach aquifers subjected to tides, *Water Resources Research*, *56*(3), e2019WR026430.

Geng, X., M. C. Boufadel, and B. Wrenn (2013), Mathematical modeling of the biodegradation of residual hydrocarbon in a variably-saturated sand column, *Biodegradation*, *24*(2), 153-163.

Geng, X., M. C. Boufadel, Y. Xia, H. Li, L. Zhao, N. L. Jackson, and R. S. Miller (2014b), Numerical study of wave effects on groundwater flow and solute transport in a laboratory beach, *Journal of contaminant hydrology*, *165*, 37-52.

Geng, X., J. W. Heiss, H. A. Michael, and M. C. Boufadel (2017b), Subsurface flow and moisture dynamics in response to swash motions: Effects of beach hydraulic conductivity and capillarity, *Water Resources Research*, *53*(12), 10317-10335.

Geng, X., J. W. Heiss, H. A. Michael, H. Li, B. Raubenheimer, and M. C. Boufadel (2021b), Geochemical fluxes across the land-sea interface through sandy coastlines: Modulation due to major physical stressors and geological heterogeneity, *Earth-Science Reviews*, *accepted*.

Geng, X., Z. Pan, M. C. Boufadel, T. Ozgokmen, K. Lee, and L. Zhao (2016), Simulation of oil bioremediation in a tidally influenced beach: Spatiotemporal evolution of nutrient and dissolved oxygen, *Journal of Geophysical Research: Oceans*, *121*(4), 2385-2404.

Giblin, A. E., K. H. Foreman, and G. T. Banta (1995), Biogeochemical processes and marine benthic community structure: which follows which?, in *Linking Species & Ecosystems*, edited, pp. 37-44, Springer.

Glemarec, M., and E. Hussenot (1981), Définition d'une succession écologique en milieu meuble anormalement enrichi en matières organiques à la suite de la catastrophe de l'AMOCO CADIZ, paper presented at Proceedings of International Symposium on the Amoco Cadiz, Fate and Effects of the Oil Spill. CNEXO, Brest, France.

Glud, R. N., S. Forster, and M. Huettel (1996), Influence of radial pressure gradients on solute exchange in stirred benthic chambers, *Marine Ecology Progress Series*, *141*, 303-311.

Gong, Y., X. Zhao, Z. Cai, S. O'reilly, X. Hao, and D. Zhao (2014), A review of oil, dispersed oil and sediment interactions in the aquatic environment: influence on the fate, transport and remediation of oil spills, *Marine pollution bulletin*, *79*(1-2), 16-33.

Huettel, M., and G. Gust (1992), Solute release mechanisms from confined sediment cores in stirred benthic chambers and flume flows, *Marine ecology progress series. Oldendorf*, *82*(2), 187-197.

Huettel, M., W. Ziebis, S. Forster, and G. Luther Iii (1998), Advective transport affecting metal and nutrient distributions and interfacial fluxes in permeable sediments, *Geochimica et Cosmochimica Acta*, *62*(4), 613-631.

Janssen, F., P. Faerber, M. Huettel, V. Meyer, and U. Witte (2005a), Pore-water advection and solute fluxes in permeable marine sediments (I): Calibration and performance of the novel benthic chamber system Sandy, *Limnology and Oceanography*, *50*(3), 768-778.

Janssen, F., M. Huettel, and U. Witte (2005b), Pore-water advection and solute fluxes in permeable marine sediments (II): Benthic respiration at three sandy sites with different

permeabilities (German Bight, North Sea), *Limnology and Oceanography*, *50*(3), 779-792.
Khalili, A., A. Basu, and M. Huettel (1997), A non-Darcy model for recirculating flow through a fluid-sediment interface in a cylindrical container, *Acta Mechanica*, *123*(1), 75-87.
Khalili, A., A. Basu, U. Pietrzyk, and B. B. Jørgensen (1999), Advective transport through permeable sediments: a new numerical and experimental approach, *Acta mechanica*, *132*(1), 221-227.
McCay, D. P. F., C.-A. Manen, M. Gibson, and J. Catena (2001), Quantifying the Scale of Restoration Required to Compensate for the Impacts of the North Cape Oil Spill on Fish and Invertebrates, paper presented at International Oil Spill Conference, American Petroleum Institute.
Meysman, F. J., O. S. Galaktionov, P. L. Cook, F. Janssen, M. Huettel, and J. J. Middelburg (2007), Quantifying biologically and physically induced flow and tracer dynamics in permeable sediments, *Biogeosciences*, *4*(4), 627-646.
Michel, J., and M. O. Hayes (1999), Weathering patterns of oil residues eight years after the Exxon Valdez oil spill, *Marine pollution bulletin*, *38*(10), 855-863.
Michel, J., E. H. Owens, S. Zengel, A. Graham, Z. Nixon, T. Allard, W. Holton, P. D. Reimer, A. Lamarche, and M. White (2013), Extent and degree of shoreline oiling: Deepwater Horizon oil spill, Gulf of Mexico, USA, *PloS one*, *8*(6), e65087.
Montagna, P. A., J. G. Baguley, C. Cooksey, I. Hartwell, L. J. Hyde, J. L. Hyland, R. D. Kalke, L. M. Kracker, M. Reuscher, and A. C. Rhodes (2013), Deep-sea benthic footprint of the Deepwater Horizon blowout, *PloS one*, *8*(8), e70540.
Neff, J. M. (2002), *Bioaccumulation in marine organisms: effect of contaminants from oil well produced water*, Elsevier.
O'Laughlin, C. M., B. A. Law, V. S. Zions, T. L. King, B. Robinson, and Y. Wu (2017), Settling of dilbit-derived oil-mineral aggregates (OMAs) & transport parameters for oil spill modelling, *Marine pollution bulletin*, *124*(1), 292-302.
Owens, E. H., and K. Lee (2003), Interaction of oil and mineral fines on shorelines: review and assessment, *Marine pollution bulletin*, *47*(9-12), 397-405.
Passow, U., and E. B. Overton (2021), The complexity of spills: the fate of the Deepwater Horizon oil, *Annual Review of Marine Science*, *13*, 109-136.
Reuscher, M. G., J. G. Baguley, N. Conrad-Forrest, C. Cooksey, J. L. Hyland, C. Lewis, P. A. Montagna, R. W. Ricker, M. Rohal, and T. Washburn (2017), Temporal patterns of Deepwater Horizon impacts on the benthic infauna of the northern Gulf of Mexico continental slope, *PloS one*, *12*(6), e0179923.
Rocha, C. (2008), Sandy sediments as active biogeochemical reactors: compound cycling in the fast lane, *Aquatic Microbial Ecology*, *53*(1), 119-127.
Santos, I. R., W. C. Burnett, T. Dittmar, I. G. Suryaputra, and J. Chanton (2009), Tidal pumping drives nutrient and dissolved organic matter dynamics in a Gulf of Mexico subterranean estuary, *Geochimica et Cosmochimica Acta*, *73*(5), 1325-1339.
Shan, J., J. Wang, J. Zhan, L. Liu, F. Wu, and X. Wang (2020), Sorption behaviors of crude oil on polyethylene microplastics in seawater and digestive tract under simulated real-world conditions, *Chemosphere*, *257*, 127225.
Short, J. W., M. R. Lindeberg, P. M. Harris, J. M. Maselko, J. J. Pella, and S. D. Rice (2004), Estimate of oil persisting on the beaches of Prince William Sound 12 years after the Exxon

625 Valdez oil spill, *Environmental science & technology*, *38*(1), 19-25.
626 Shum, K. (1992), Wave-induced advective transport below a rippled water-sediment
627 interface, *Journal of Geophysical Research: Oceans*, *97*(C1), 789-808.
628 Teal, J. M., and R. W. Howarth (1984), Oil spill studies: a review of ecological effects,
629 *Environmental Management*, *8*(1), 27-43.
630 Tengberg, A., F. De Bovee, P. Hall, W. Berelson, D. Chadwick, G. Ciceri, P. Crassous, A.
631 Devol, S. Emerson, and J. Gage (1995), Benthic chamber and profiling landers in
632 oceanography—a review of design, technical solutions and functioning, *Progress in*
633 *Oceanography*, *35*(3), 253-294.
634 Thrift-Viveros, D. L., R. Jones, and M. Boufadel (2015), Development of a new oil
635 biodegradation algorithm for NOAA's oil spill modelling suite (GNOME/ADIOS), paper
636 presented at Proceedings of the Thirty-Eighth AMOP Technical Seminar, Vancouver, BC,
637 Canada.
638 Wang, S., D. Wang, Z. Yu, X. Dong, S. Liu, H. Cui, and B. Sun (2021), Advances in research
639 on petroleum biodegradability in soil, *Environmental Science: Processes & Impacts*, *23*(1), 9-
640 27.
641 Webb, J. E., and J. Theodor (1968), Irrigation of submerged marine sands through wave
642 action, *Nature*, *220*(5168), 682-683.
643 Werner, U., P. Bird, C. Wild, T. Ferdelman, L. Polerecky, G. Eickert, R. Jonstone, O. Hoegh-
644 Guldberg, and D. de Beer (2006), Spatial patterns of aerobic and anaerobic mineralization
645 rates and oxygen penetration dynamics in coral reef sediments, *Marine Ecology Progress*
646 *Series*, *309*, 93-105.
647 Zheng, C., and G. D. Bennett (2002), *Applied Contaminant Transport Modelling*, John Wiley
648 and Sons, New York, USA.

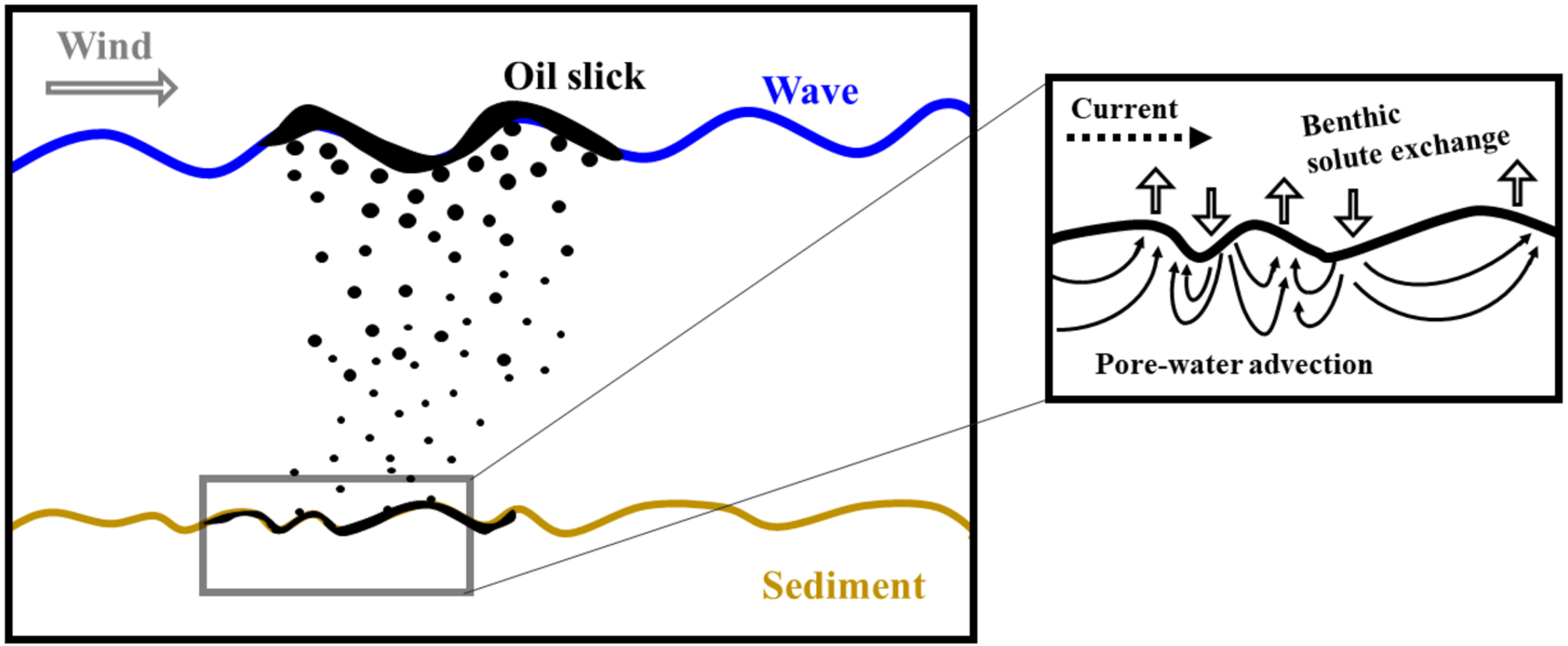
Wind
Oil slick
Wave
Sediment
Current
Benthic
solute exchange
Pore-water advection

(A)

Basu and Khalili (1999), simulated

CYL-BIOMARUN, simulated

radioactivity strength

0.0 - 0.1
0.1 - 0.2
0.2 - 0.3
0.3 - 0.4
0.4 - 0.5
0.5 - 0.6
0.6 - 0.7
0.7 - 0.8
0.8 - 0.9
0.9 - 1.0

Time t = 0.5 h | t = 1.0 h | t = 1.5 h | t = 2.0 h

Elevation, cm

Distance, cm

(B)

Khalili et al., (1999)

Basu and Khalili (1999)

CYL-BIOMARUN, simulated

Washout depth, cm

Time, min

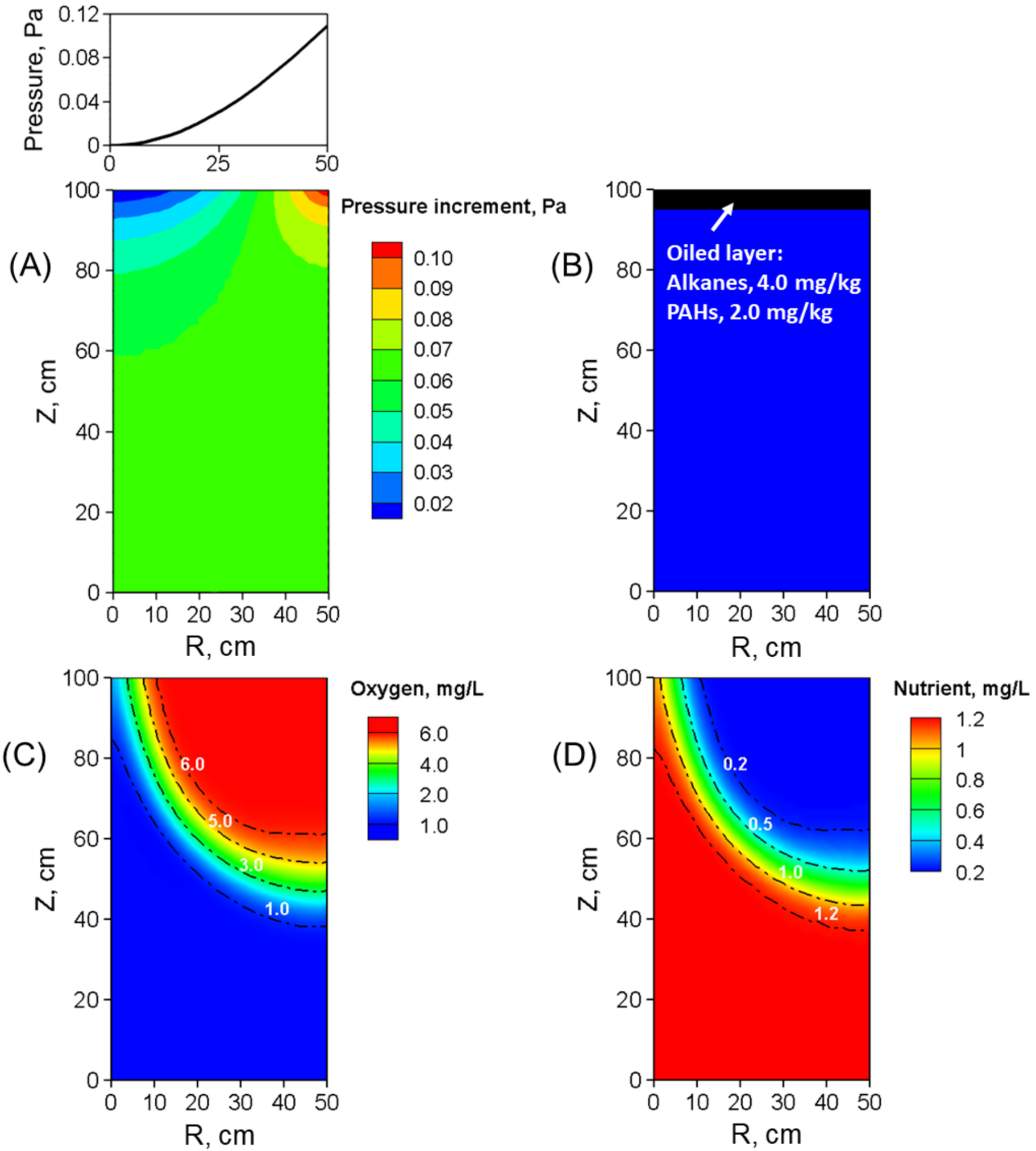
Pressure, Pa
0.12
0.08
0.04
0
0
25
50
(A)
Pressure increment, Pa
0.10
0.09
0.08
0.07
0.06
0.05
0.04
0.03
0.02
Z, cm
R, cm
(B)
Oiled layer:
Alkanes, 4.0 mg/kg
PAHs, 2.0 mg/kg
(C)
Oxygen, mg/L
6.0
4.0
2.0
1.0
6.0
5.0
3.0
1.0
(D)
Nutrient, mg/L
1.2
1
0.8
0.6
0.4
0.2
0.2
0.5
1.0
1.2

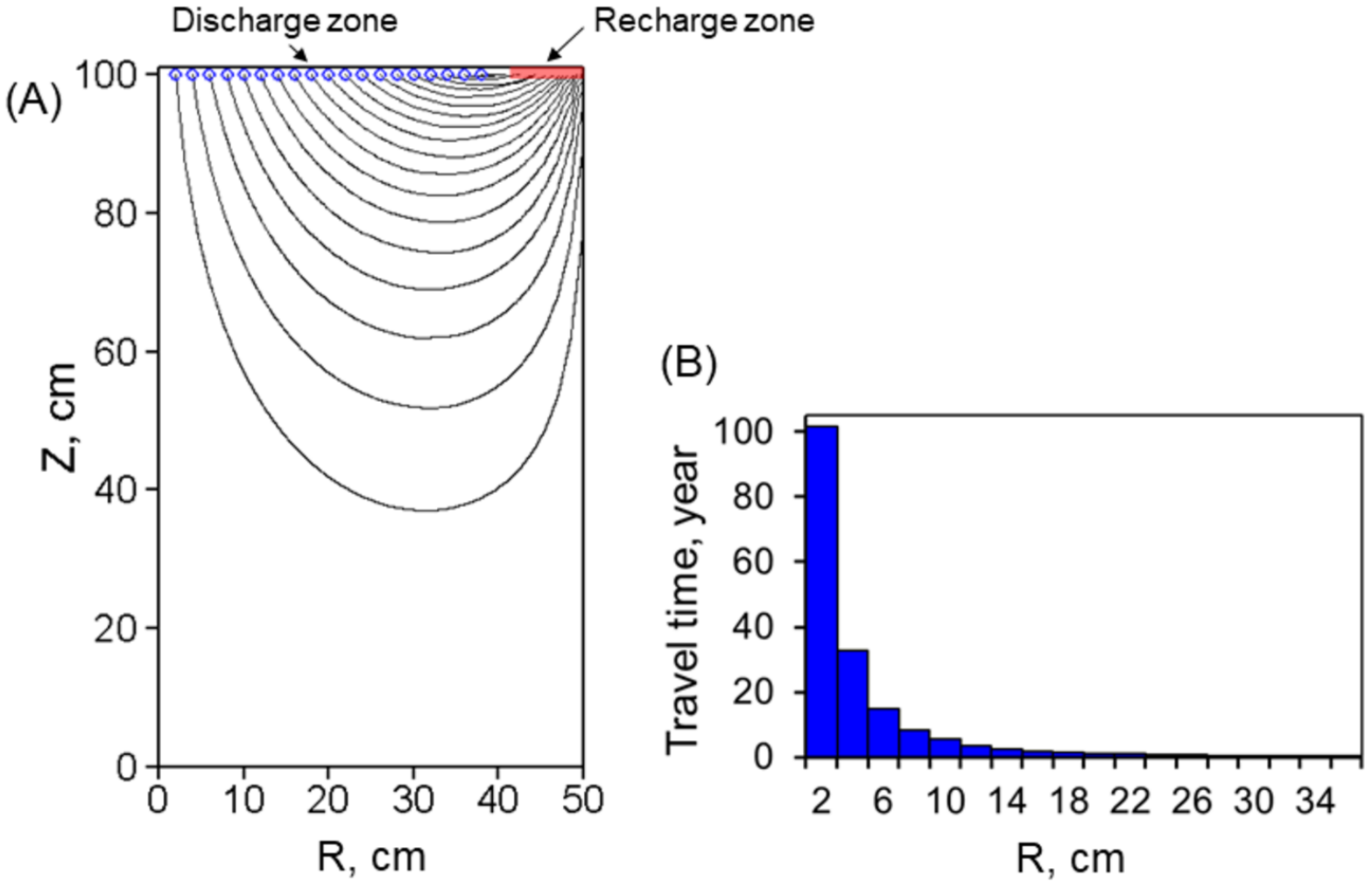
Discharge zone
Recharge zone
(A)
Z, cm
R, cm
0
20
40
60
80
100
0
10
20
30
40
50
(B)
Travel time, year
R, cm
0
20
40
60
80
100
2
6
10
14
18
22
26
30
34

time t = 30 days
t = 60 days
t = 100 days
t = 300 days

Alkanes, mg/kg

(A)

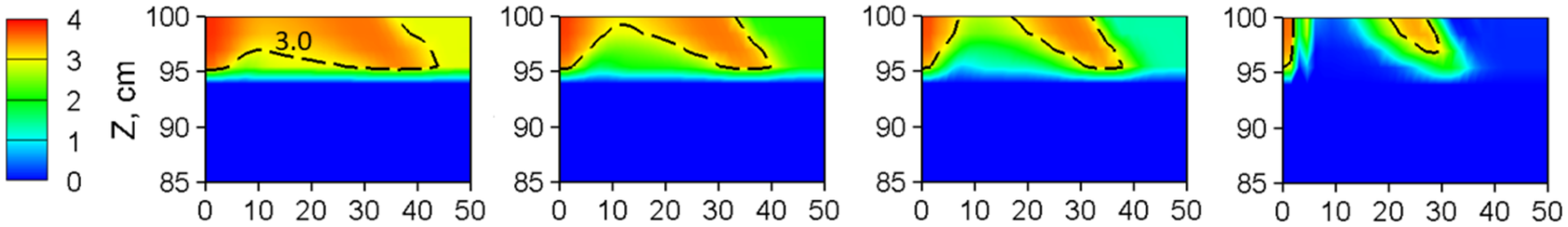


PAHs, mg/kg

(B)

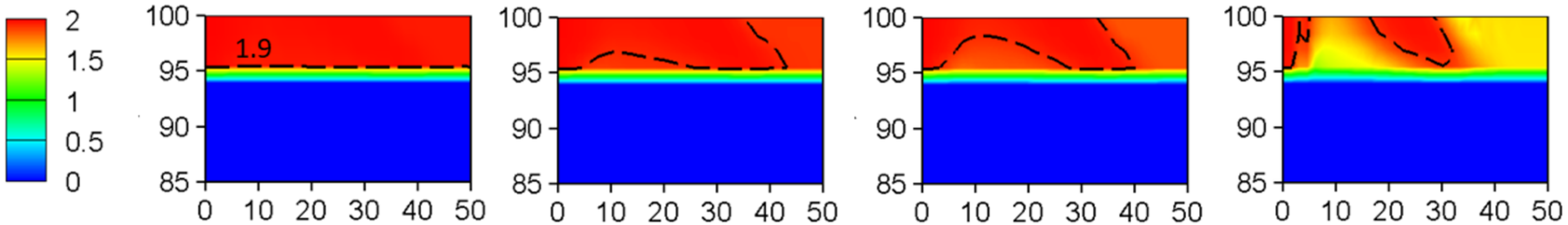


Oxygen, mg/L

(C)

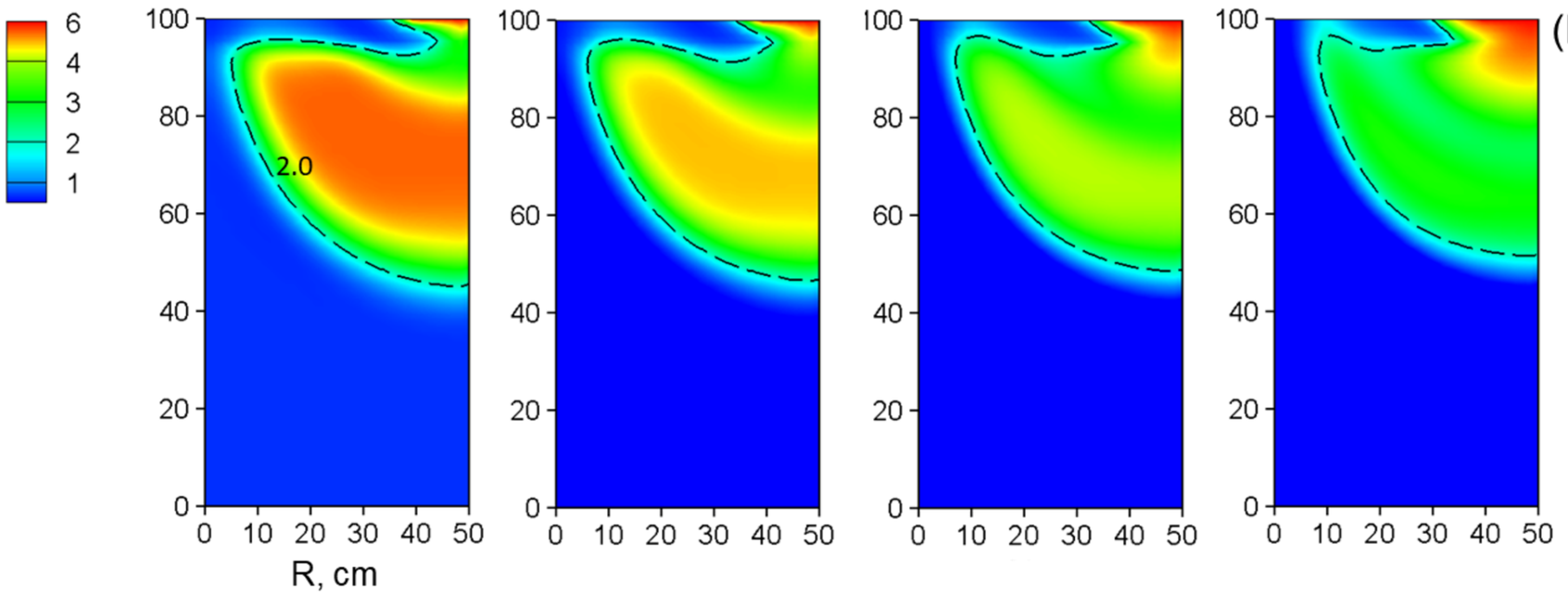


t = 300 days

Nutrient, mg/L

(D)

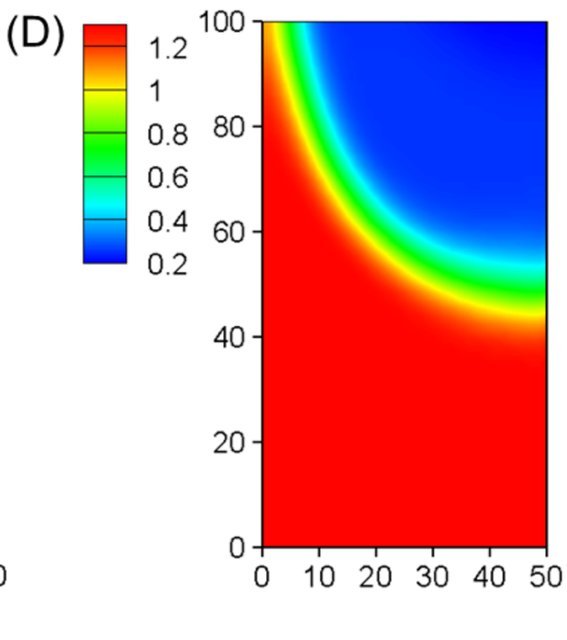

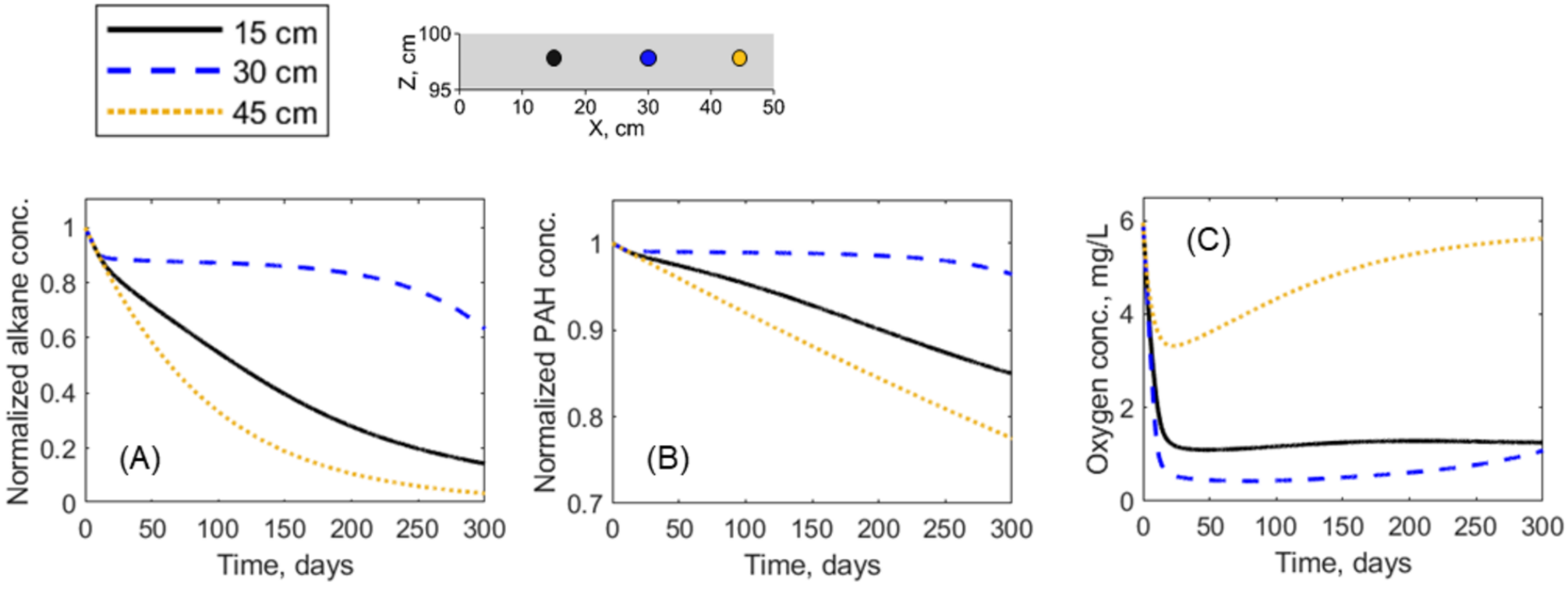
15 cm
30 cm
45 cm
Z, cm
100
95
0
10
20
30
40
50
X, cm
Normalized alkane conc.
(A)
Time, days
Normalized PAH conc.
(B)
Time, days
Oxygen conc., mg/L
(C)
Time, days

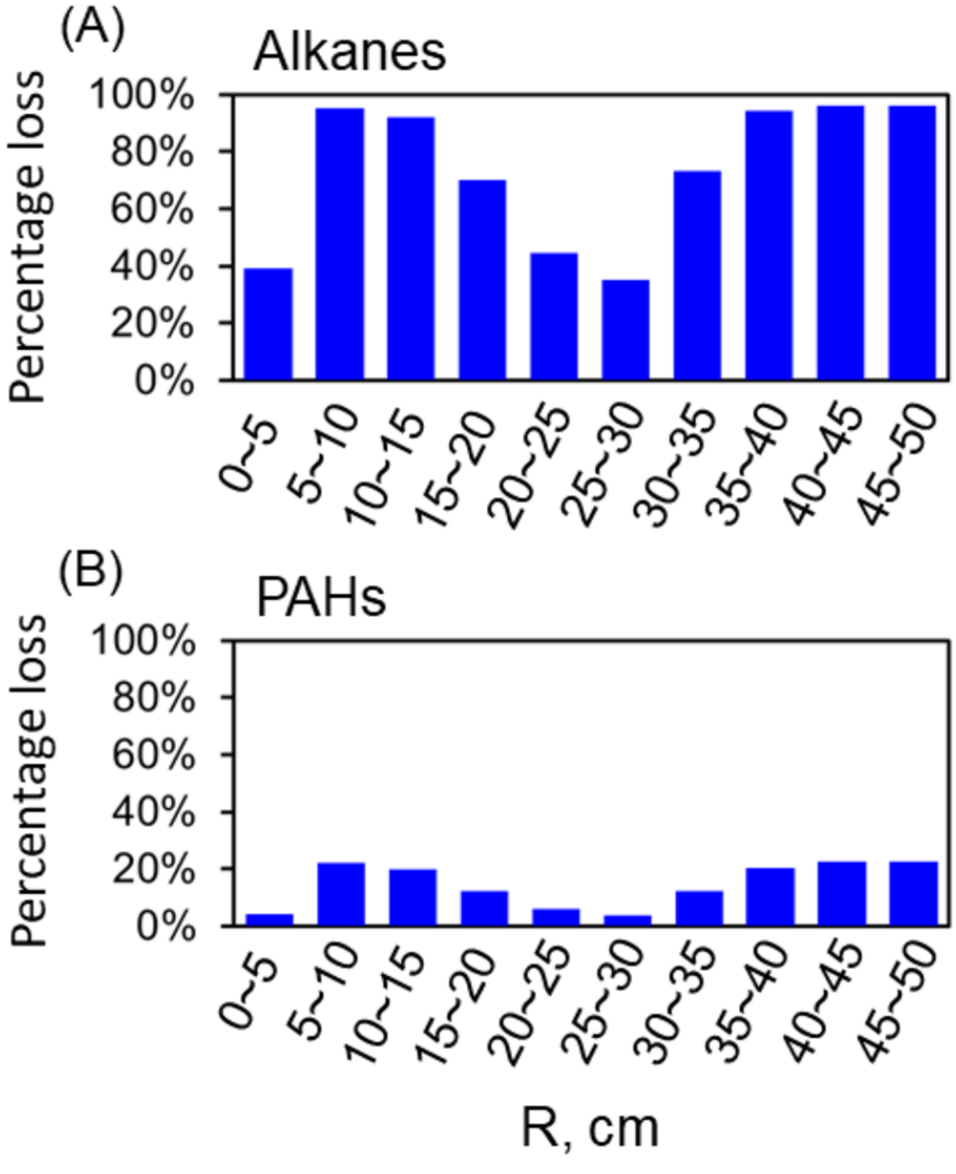
(A)
Alkanes
Percentage loss
100%
80%
60%
40%
20%
0%
0~5
5~10
10~15
15~20
20~25
25~30
30~35
35~40
40~45
45~50
(B)
PAHs
Percentage loss
100%
80%
60%
40%
20%
0%
0~5
5~10
10~15
15~20
20~25
25~30
30~35
35~40
40~45
45~50
R, cm

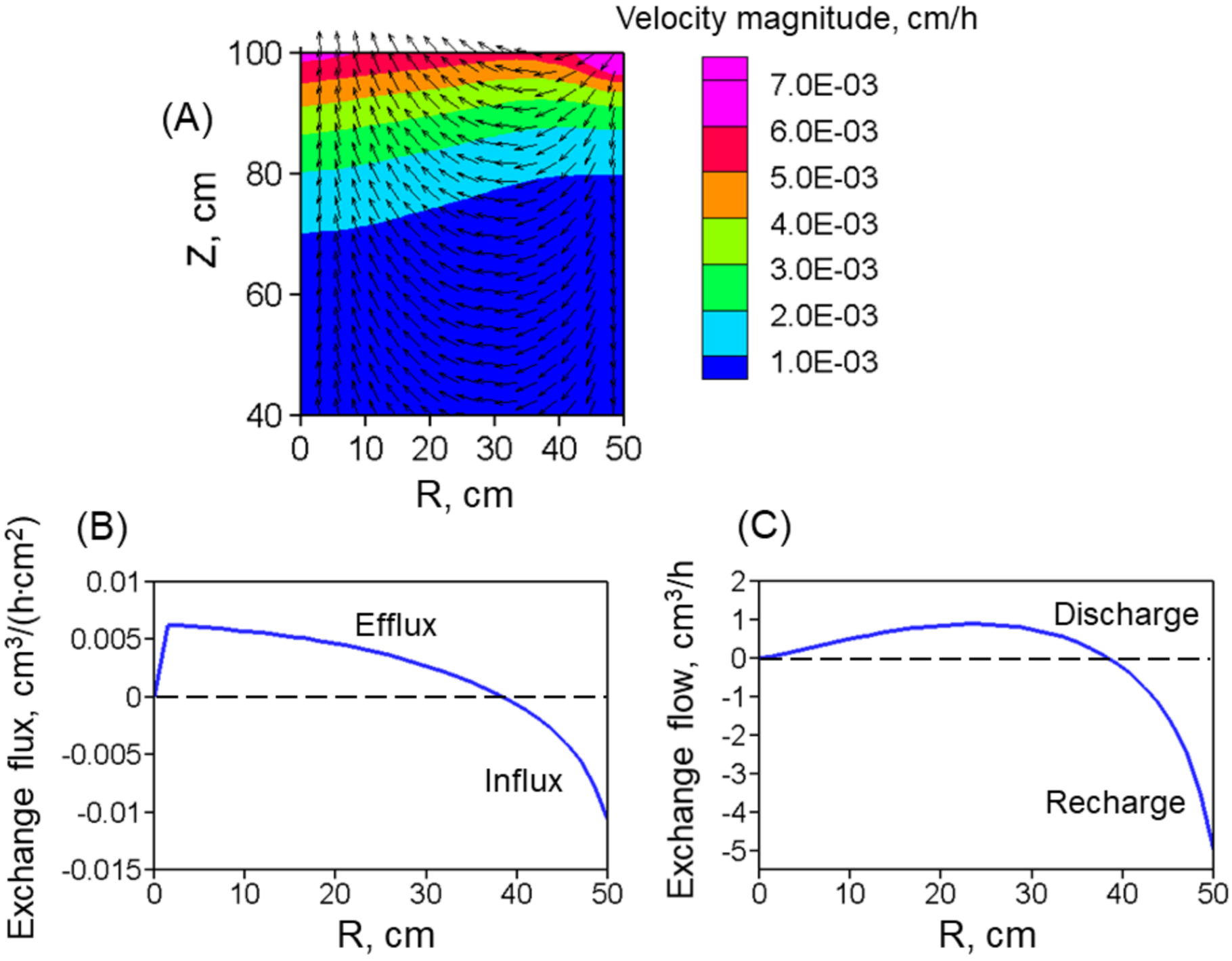
(A)
Velocity magnitude, cm/h
7.0E-03
6.0E-03
5.0E-03
4.0E-03
3.0E-03
2.0E-03
1.0E-03
Z, cm
R, cm
100
80
60
40
0
10
20
30
40
50
(B)
Exchange flux, cm³/(h·cm²)
Efflux
Influx
0.01
0.005
0
-0.005
-0.01
-0.015
R, cm
(C)
Exchange flow, cm³/h
Discharge
Recharge
2
1
0
-1
-2
-3
-4
-5
R, cm

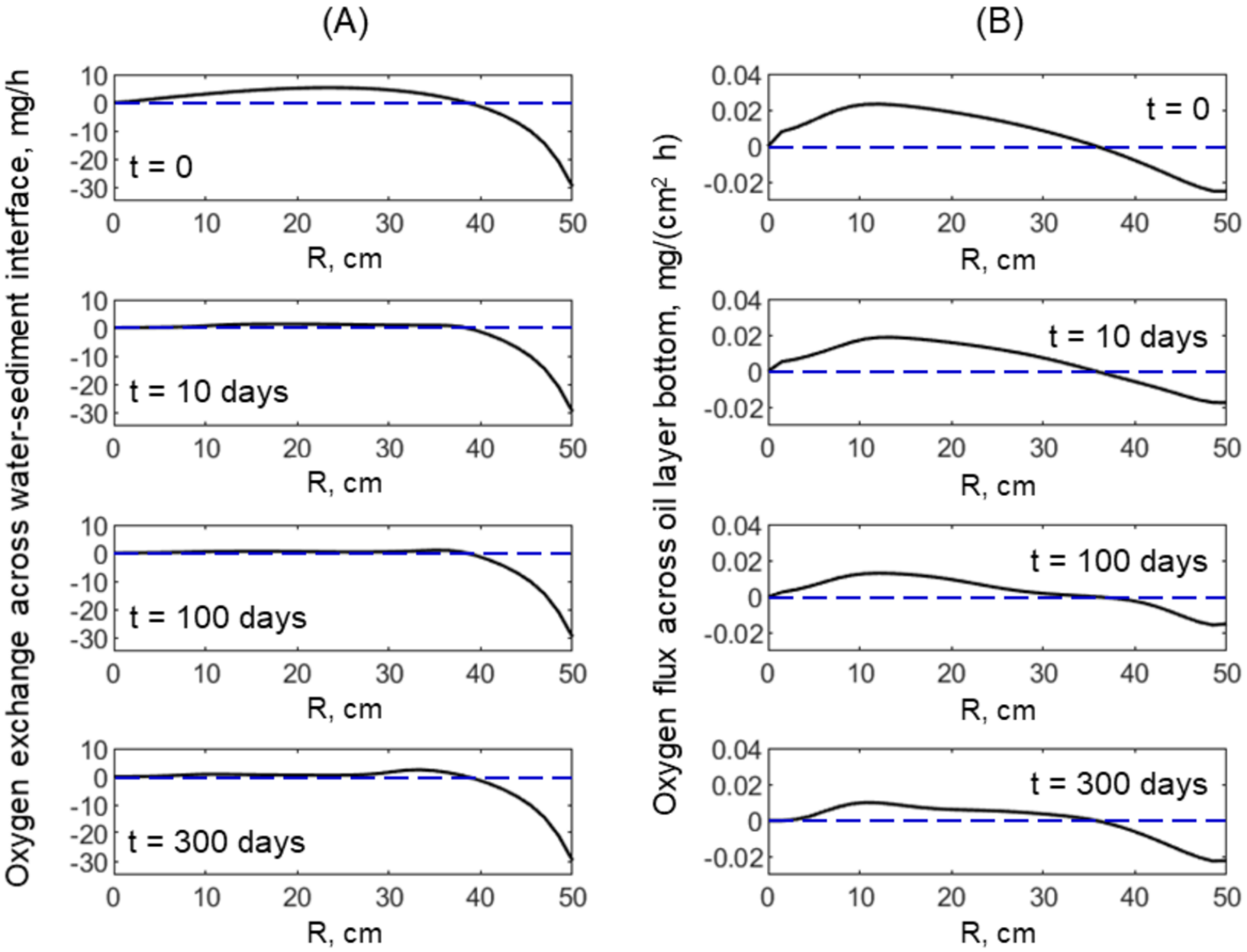
(A)
(B)
Oxygen exchange across water-sediment interface, mg/h
Oxygen flux across oil layer bottom, mg/(cm² h)
t = 0
t = 10 days
t = 100 days
t = 300 days
R, cm
10
0
-10
-20
-30
0.04
0.02
0
-0.02
0
10
20
30
40
50

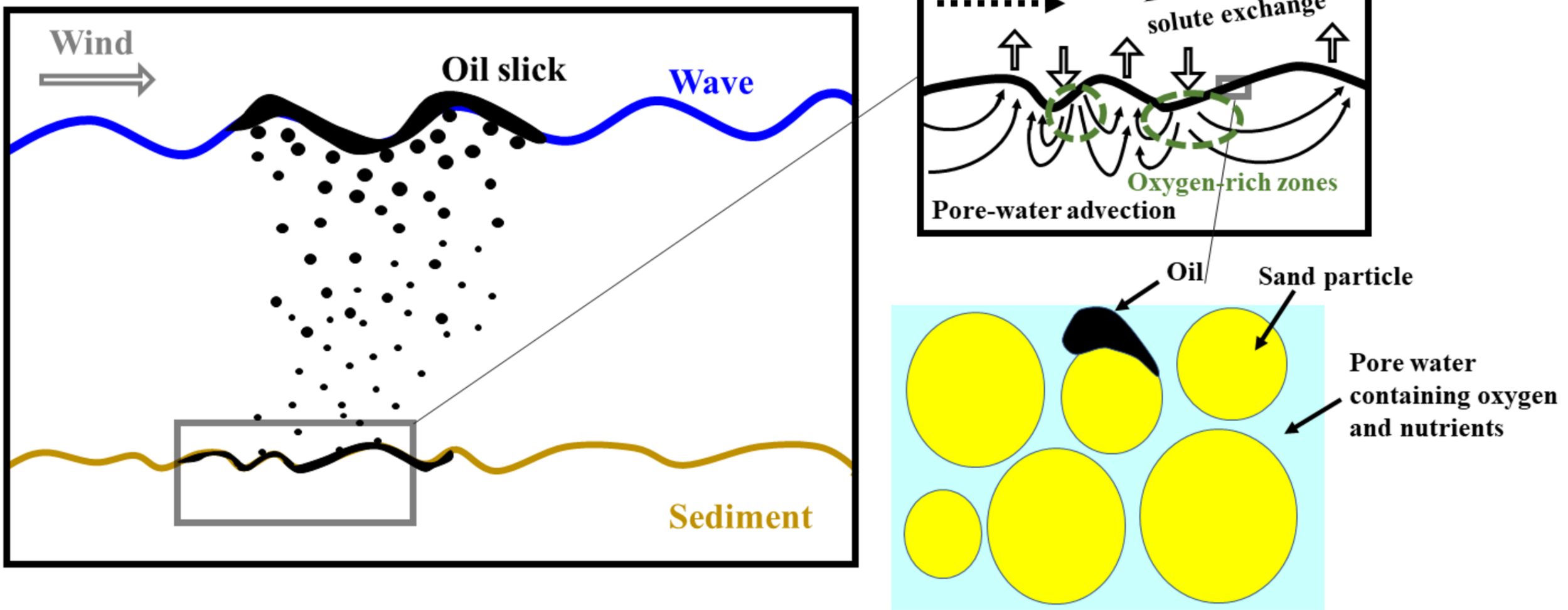
Wind
Oil slick
Wave
Sediment
Current
Benthic
solute exchange
Oxygen-rich zones
Pore-water advection
Oil
Sand particle
Pore water
containing oxygen
and nutrients